Published in final edited form as:
Circulation. 2005 September 6; 112(10): 1451–1461.

Dynamic Imaging of Allogeneic Mesenchymal Stem Cells Trafficking to Myocardial Infarction

Dara L. Kraitchman, VMD, PhD, **Mitsuaki Tatsumi, MD, PhD**, **Wesley D. Gilson, PhD**, **Takayoshi Ishimori, MD, PhD**, **Dorota Kedziorek, MD**, **Piotr Walczak, MD**, **W. Paul Segars, PhD**, **Hunter H. Chen, MSE**, **Danielle Fritzges, AA**, **Izlem Izbudak, MD**, **Randell G. Young, DVM**, **Michelle Marcelino, BS**, **Mark F. Pittenger, PhD**, **Meiyappan Solaiyappan, MS**, **Raymond C. Boston, PhD**, **Benjamin M.W. Tsui, PhD**, **Richard L. Wahl, MD**, and **Jeff W.M. Bulte, PhD**
From the Russell H. Morgan Department of Radiology and Radiological Science (D.L.K., M.T., W.D.G., T.I., D.K., P.W., W.P.S., H.H.C., D.F., I.I., M.S., B.M.W.T., R.L.W., J.W.M.B.) and Institute for Cell Engineering (D.K., P.W., J.W.M.B.), Johns Hopkins University School of Medicine, Baltimore, Md; Osiris Therapeutics, Inc, Baltimore, Md (R.G.Y., M.M., M.F.P.); and School of Veterinary Medicine, University of Pennsylvania, Kennett Square, Pa (R.C.B.).

Abstract

Background—Recent results from animal studies suggest that stem cells may be able to home to sites of myocardial injury to assist in tissue regeneration. However, the histological interpretation of postmortem tissue, on which many of these studies are based, has recently been widely debated.

Methods and Results—With the use of the high sensitivity of a combined single-photon emission CT (SPECT)/CT scanner, the in vivo trafficking of allogeneic mesenchymal stem cells (MSCs) colabeled with a radiotracer and MR contrast agent to acute myocardial infarction was dynamically determined. Redistribution of the labeled MSCs after intravenous injection from initial localization in the lungs to nontarget organs such as the liver, kidney, and spleen was observed within 24 to 48 hours after injection. Focal and diffuse uptake of MSCs in the infarcted myocardium was already visible in SPECT/CT images in the first 24 hours after injection and persisted until 7 days after injection and was validated by tissue counts of radioactivity. In contrast, MRI was unable to demonstrate targeted cardiac localization of MSCs in part because of the lower sensitivity of MRI.

Conclusions—Noninvasive radionuclide imaging is well suited to dynamically track the biodistribution and trafficking of mesenchymal stem cells to both target and nontarget organs.

Keywords

magnetic resonance imaging; myocardial infarction; nuclear medicine; radionuclide imaging; stem cell

Correspondence to Dr Dara L. Kraitchman, Johns Hopkins University, 601 N Caroline St, JHOC 4231, Baltimore, MD 21287. E-mail dara@mri.jhu.edu.

Disclosure

Michelle Marcelino, Randell Young, and Mark Pittenger are employees of and have minor ownership interests in Osiris Therapeutics, Inc, which has a commercial interest in the development of mesenchymal stem cell therapies. Dr Kraitchman has received a research grant from Osiris Therapeutics and other research support from the National Institutes of Health. Dr Tsui is the principal investigator on a research contract from GE Healthcare and is co-licensor of a software package to GE Healthcare. Dr Wahl has received a research grant from GE Healthcare and has served on the speakers' bureaus of and/or received honoraria from Cardinal Health, GE Healthcare, and Philips Medical. Dr Bulte has received research support from Osiris Therapeutics, Inc.

The online-only Data Supplement, which contains 2 additional figures and 6 movies, can be found at http://circ.ahajournals.org/cgi/content/full/CIRCULATIONAHA.105.537480/DC1.

Because of the limited regenerative capacity of the heart, stem cell transplantation is now being explored as a new method to limit infarct size and prevent deleterious remodeling after myocardial infarction (MI).[1–8] The success of such therapies in patients will require methods to determine the biodistribution and fate of stem cells without postmortem histology as well as noninvasive imaging techniques as a measure of cardiac function to determine stem cell therapy efficacy.[3,9,10]

Gender-mismatch heart transplantation has shown the ability of certain host cells, presumably bone marrow–derived mesenchymal stem cells (MSCs), to migrate into the heart.[11–16] With this in mind, many investigators have administered intravenously cell preparations containing stem cells to potentially augment the pool of endogenous stem cells homing to the myocardium after infarction. However, the localization of these exogenous cells in the infarcted tissue has relied primarily on postmortem histology, and the dynamic redistribution of peripherally injected stem cells as well as trafficking of cells could only be surmised by comparative studies with serial sacrifice of large numbers of animals.

MSCs isolated from bone marrow have the ability to differentiate into multiple cell lineages including osteocytes, chondrocytes, and cardiac myocytes.[17,18] Moreover, because MSCs can be culture-expanded in large numbers, the potential exists to deliver a substantial quantity of MSCs to repair or reconstitute a wide array of organs including the heart. The recent ability to label MSCs with radiotracers[19–21] provides a method to serially assess the biodistribution of these stem cells after intravenous administration with the use of radio-nuclide imaging as well as to determine the homing potential of MSCs to sites of injury.

^{111}In oxine labeling is a commercially available radioactive tracer used clinically to label leukocytes for monitoring inflammation. ^{111}In oxine labeling using many different types of cells across different species can be readily tagged. In addition, ^{111}In oxine is an attractive labeling agent because of the relatively long half-life at 67.3 hours, which allows for prolonged serial, dynamic imaging.

We present here combined single-photon emission CT (SPECT) and x-ray CT (SPECT/CT) and MRI studies of intravenous delivery of ^{111}In oxine–labeled MSCs colabeled with ferumoxides–poly-L-lysine (PLL) in a large-animal model of acute MI. The biodistribution of the radiolabeled MSCs was assessed immediately after injection as well as at multiple time points between 1 and 7 days after injection to determine MSC redistribution and the homing potential of MSCs to damaged cardiac tissue.

Methods

MSC Culture and Labeling

Canine MSCs were isolated from iliac crest bone marrow, culture-expanded for 2 passages in vitro, and frozen, as described previously.[17] After thawing, magnetic labeling of the MSCs was achieved by 24-hour incubation in culture medium containing a ferumoxides injectable solution (25 μg Fe per milliliter, Feridex, Berlex Laboratories) mixed with PLL (375 ng/mL; average molecular weight, 275 kDa) 1 hour before cell incubation.[22,23] The MSCs were washed and labeled with a fluorescent marker (Cell Tracker Orange, Molecular Probes) for fluorescence analysis of histological samples in conjunction with immunofluorescent staining.

For radiolabeling, the Feridex-PLL fluorescently labeled MSCs were first washed with PBS, mixed, and suspended with ^{111}In oxine and then were incubated for 20 minutes at room temperature with 769 ± 268 μCi ^{111}In oxine. Cells were centrifuged at 400*g* for 7 minutes, and the supernatant was removed. The cells were then washed with Hanks' balanced salt solution (Sigma Chemical Co) and again centrifuged at 320*g* for 7 minutes. After the aforementioned

cell washing was repeated, the ^{111}In oxine radiolabeling efficiency of the MSC was measured, and cell viability was determined by trypan blue exclusion.

In Vitro Proliferation, Toxicity, and Differentiation Assays

To determine the dose-response toxicity of MSCs to ^{111}In oxine labeling, aliquots of 2×10^7 canine MSCs from a single donor were labeled with increasing dosages of radiotracer (ie, 0, 5, 10, 20, and 30 μCi per million MSCs) with the use of the previously described labeling protocol. Serial measurements of cell counts and radioactivity were performed on alternate days in alternate flasks that were initially seeded with 2 million viable MSCs per T-25 flask. In addition, immediately after labeling and at 1, 2, 3, 6, and 8 days after labeling, cell viability was determined by trypan blue exclusion, and metabolic activity/proliferation rate was determined by (3-(4,5-dimethylthiazol-2-yl)-5-(3-carboxymethoxyphenyl)-2-(4-sulfophenyl)-2H-tetrazolium, inner salt) (MTS) assay.[24]

The MTS assay (Promega) was performed at each time point in triplicate, with 5000 MSCs plated per 100-μL well in a 96-well plate, which was incubated at 37°C for 2 hours followed by absorbance measurements at 492 nm with the use of a microplate reader (Beckman Coulter). Media changes were performed after 4 days for the well plates that were tested at >4 days. Absorbance measurements for the different radiolabeled doses of MSC were compared with unlabeled MSCs by a linear regression analysis.

The ability of the MSCs to differentiate into normal adipocytes was determined at all labeling doses. Approximately 2×10^5 MSCs were plated per well of a 24-well plate, and the cells were allowed to form a confluent monolayer. The MSCs were then subjected to 3 cycles of induction with adipogenic induction medium (Cambrex) and maintenance in maintenance medium (Cambrex) with the use of a standard protocol[25] to stimulate adipogenic differentiation. After the third cycle, cells were held in maintenance medium for 7 days. At harvest, the medium was gently aspirated, and the cells were fixed in 10% buffered formalin and stained with Oil Red O. Only cells with neutral lipid vacuoles appear red, indicating adipogenic differentiation.

Experimental Protocol

The studies were approved and conducted in accordance with the institutional guidelines for care of laboratory animals. Mongrel dogs (weight, 25 to 30 kg) were induced with sodium thiopental, intubated, and placed on isoflurane anesthesia with mechanical ventilation for the duration of the surgical procedure. To create an acute nontransmural MI, a 90-minute closed-chest left anterior descending coronary artery balloon occlusion with the use of x-ray cardiac catheterization techniques, followed by reperfusion, as described previously,[20] was performed in 7 dogs. At 72 hours after reperfusion, 6 animals were reanesthetized and received $1.6 \times 10^{8\pm}$ 2.1×10^7 Feridex-PLL ^{111}In oxine–labeled MSCs intravenously, followed immediately by SPECT/CT imaging. In 1 animal not subjected to balloon occlusion and reperfusion, 9.8×10^7 Feridex-PLL ^{111}In oxine–labeled MSCs were administered intravenously, followed immediately by SPECT/CT imaging. In 1 animal subjected to experimental MI, ^{111}In oxine (1.1 mCi) without MSCs was administered intravenously, followed immediately by SPECT/CT imaging.

SPECT/CT Imaging Protocol

The anesthetized dogs were mechanically ventilated and placed in left decubitus. Serial SPECT/CT projection data were acquired on a clinical scanner (Millenium VG/Hawkeye, GE Healthcare) immediately after injection (day 1), at 24 hours after injection (day 2), and at at least 1 time point between 48 to 168 hours after injection (day 3 to day 8) to determine the initial distribution and dynamic redistribution of the MSCs versus ^{111}In oxine. Two imaging sections were acquired to obtain whole-body images of the thorax and abdomen. Imaging

parameters were as follows: medium energy collimators, 128 × 128 projection matrix, 3.45-mm pixel, 120 projections over a 360-degree rotation with the use of dual cameras, and 30 to 60 seconds for each projection (depending on the imaging day after injection). Two energy windows were acquired around the 173 and 247 keV ^{111}In photopeaks.

SPECT/CT Image Reconstruction and Analysis

The acquired SPECT and CT data were processed with the use of a custom software package. The quantitative image reconstruction method consists of a 3-dimensional (3D) iterative ordered-subset expectation-maximization algorithm (5 iterations with 10 subsets) and a projector and back-projector pair that models image degradation factors including nonuniform attenuation[26] and scatter[27] of photons within the animal and the full collimator-detector response[28] with the medium energy collimator for their accurate compensation[29,30] to obtain higher image resolution and less noise compared with the conventional filtered back-projection reconstruction method. The registered CT images were used for nonuniform attenuation distribution within the animal's body.

The fused SPECT/CT images were examined visually in the transaxial, sagittal, and coronal planes for ^{111}In oxine uptake in major organs as well as redistribution over time. The mean pixel values in 3D regions of interest (ROIs) in the lung, heart, kidney, spleen, liver, and spine were defined on the 3 plane views with a custom tool (Amide31) for each imaging session. Elliptical ROIs were chosen such that they sampled as large a volume of the organ as possible without creating partial volume errors. The ROI volume for each organ was kept constant between imaging sessions for each animal. Emission data for each imaging session were normalized for counts per projection and expressed as a percentage of left lung uptake immediately after intravenous MSC injection. ROI data were plotted by organ over time, where the logarithm of the emission data over time would be expected to be linear only if radioactive decay of tissue uptake was occurring.

Whole-body emission counts from the 3D ROIs were determined at each imaging session for all animals. In addition, emission counts for known amounts of ^{111}In oxine radioactivity that were placed on the chest wall of the animal that received only radiotracer without MSCs were determined. With the use of the emission counts per second of the known ^{111}In oxine standards, the expected injected dose was determined for each animal on the day of injection and compared with the actual injected dose. In addition, the whole-body emission counts were decay-corrected, and the percentage of the original dose that could be accounted for was determined at each successive imaging session.

Statistical Analysis

For comparison with postmortem tissue well counter counts, the emission data were corrected for radioactive decay between the time of imaging and well counting, and a robust regression (Stata Corporation) was performed with clustering by animal. Statistically significant differences in cell viability and toxicity assays by day or labeling dose were determined by a linear regression analysis. A paired *t* test was used to compare SPECT cardiac emission data between tissues (eg, infarcted versus noninfarcted). A probability value <0.05 was considered statistically significant. All values are presented as mean ± SD.

MRI Protocol

Cardiac MRIs were obtained with the animals under general anesthesia after the final SPECT/CT study on a clinical 1.5-T MR scanner (CV/i, GE Healthcare) with a 4-channel phased array. Axial scout images were obtained to determine the extent and location of the heart. Short- and long-axis images were obtained with use of a high-resolution, ECG-gated, segmented k-space, fast, gradient echo imaging pulse sequence (repetition time 9.0 ms; echo time 2.0 ms; 32 views

per segment; 512 × 512 image matrix; 28 × 21-cm field of view; 20° flip angle; 32-kHz bandwidth; 5-mm slice thickness with no gap; and number of signal averages 3 to 4), which accentuates susceptibility artifacts due to Feridex-PLL–labeled MSCs.[23] Delayed contrast-enhanced MRI at mid-diastole in the short- and long-axis imaging planes was obtained ≈15 minutes after a 0.02-mmol/kg IV bolus of gadopentetate dimeglumine (Berlex Laboratories) with an ECG-gated, segmented k-space, inversion recovery, fast gradient echo sequence (repetition time 7.2 ms; echo time 3.2 ms; 16 views per segment; 256 × 192 image matrix interpolated to 256 × 256; 25° flip angle; 32-kHz bandwidth; 8-mm slice thickness with no gap; number of signal averages 2; and inversion time 175 to 200 ms).

MR Image Analysis

MR images were transferred to a PC for analysis with a custom software tool (cine, GE Healthcare). Endocardial and epicardial borders were segmented to determine left ventricular mass. The hyperintense myocardium on the delayed contrast-enhanced MRI, which represents nonviable myocardium,[32] was determined with full-width half-maximum criteria.[33] Infarct size was normalized to left ventricular mass.

MRI Registration With SPECT/CT Images

Volumetric data sets obtained from the MRI, CT, and SPECT were volume-rendered in a colocalized manner with the use of an opacity attribute to control the voxel-selective fusion of the multimodality data set. The CT data set provided the anatomic reference for the SPECT data registration with MRI. Initially, the axial MRI scout data set was registered with the axial CT data set with the boundaries of thorax (ie, ribs and sternum) and spine used as anatomic reference indicators for goodness of registration. With the use of 3D stereoscopic viewing and interactive display with 6-degree control for position and orientation of the individual data sets (Dextroscope, Volume Interactions Pte Ltd), manual alignment of the axial CT and MRI data sets was performed with a consensus of 3 observers. After the registration of the axial MRI to the CT data set was established, the CT data were excluded from the display to provide a coregistered volume-rendered display of the SPECT and short-axis contrast-enhanced delay MRI for anatomic localization of SPECT cardiac uptake relative to infarcted myocardium.

Postmortem Analysis

After humane euthanasia at the final imaging session, the heart was harvested, sliced along the short-axis plane, and captured as a digital image. The short-axis slices were subdivided into transmural wedges. A portion of each wedge (≈300 to 800 mg) was weighed and counted in a gamma well counter for 3 minutes. Counts per minute per gram were decay corrected and reported as a percentage of the injected dose per gram of tissue.

The remainder of each heart wedge was snap-frozen for histological analysis. Tissue obtained from the liver, kidney, spleen, lung, gastrointestinal tract, skeletal muscle, and skin was also gamma counted or frozen for histological analysis. Feridex (ie, iron)-containing cells were identified by Prussian blue staining with and without 3,3′-diaminobenzidine (DAB) enhancement.[34] An acid phosphatase stain (Sigma Aldrich) to detect macrophages was performed on adjacent sections and double stained with Prussian blue without nuclear fast red counterstaining. With the use of this protocol, double-stained cells were macrophages containing iron, whereas Prussian blue–positive only cells were Feridex-labeled MSCs. With the use of an anti-dextran mouse monoclonal antibody (DX1, StemCell Technologies) and a secondary Alexa-Fluor goat anti-mouse antibody (Molecular Probes A21141), MSCs labeled exogenously with Feridex were also identified by retention of the dextran coating of the iron oxide.

Results

In Vitro Proliferation, Toxicity, and Differentiation Assays

After ^{111}In oxine labeling, viability remained high at all labeling doses (89.3 ± 2%) with a high efficiency of labeling (82.1 ± 3%), and cell counts between labeled and unlabeled cells did not vary significantly. With trypsinization at 24 hours after seeding, there was an initial loss of cells (regardless of labeling or lack of labeling), which was not unexpected because MSCs typically require 48 hours to adhere after seeding (Figure 1A). Thereafter, cells were harvested on alternate days. Up to 6 days after labeling, there was very little noticeable cell proliferation in either labeled or unlabeled cells primarily because of plating cells close to confluence.

By MTS assay, there was a slight rise in metabolic activity/proliferation in the unlabeled cells compared with the labeled cells ($P < 0.01$) at 48 hours after labeling. However, until 6 days after labeling, the metabolic activity/proliferation in the unlabeled MSCs relative to the labeled MSCs was constant. After 6 days after labeling, a slight improvement in metabolic activity was noted in the unlabeled MSCs relative to the labeled MSCs ($P < 0.001$). However, no dose-dependent changes by MTS assay or cell counts were seen between different doses of labeled cells (Figure 1B). Moreover, ^{111}In oxine–labeled MSCs underwent adipogenic differentiation as efficiently as unlabeled MSCs (Figure 2).

Labeling Efficacy and Cell Viability

The efficiency of ^{111}In oxine labeling was high in all MSC preparations (84.7 ± 11%) for in vivo injections, with an average of 73.9 ± 16% viability immediately before injection. Approximately $1.13 \times 10^{8\pm}$ 3.6×10^{7} viable MSCs (≈5×10^{6} MSCs per kilogram) were administered intravenously with an average radioactivity of 5.05 ± 1.4 μCi per million MSCs, resulting in 673 ± 368 μCi total activity per animal.

Initial Distribution of MSCs After Intravenous Injection

In agreement with previous studies,[19,20] initial uptake of the radiolabeled MSCs administered at 72 hours after MI was restricted primarily to the lungs (Figure 3A). Modest uptake by the liver and kidney (14.5 ± 15% and 16.2 ± 21% of left lung uptake, respectively) was also seen. In addition, the initial trapping of the MSCs in the pulmonary vasculature was related to local perfusion, as demonstrated by a reduction of right lung uptake by 70 ± 10% relative to left lung uptake due to animal positioning in left decubitus (Figure 3A). The initial high uptake in the lung was not due to the closed-chest infarction procedure because lung uptake was also high in a dog that did not have a MI (Figure 3B). Moreover, the SPECT emission data were related to the pattern of MSC distribution because injection of ^{111}In oxine administered without MSCs acted primarily as a blood pool agent and resulted in no substantial lung uptake immediately after injection (Figure 3C). Volume-rendered movies of the initial high uptake in infarcted and noninfarcted dogs receiving MSCs can be viewed in the online-only Data Supplement (Movies I and II, respectively).

Early Redistribution of MSCs After Intravenous Injection

SPECT/CT imaging was performed at 24 hours after MSC injection (day 2) and at least once between days 3 to 8 after injection. On day 2, left lung uptake had dropped to 9.7 ± 2% of the original uptake value (Figure 4A). Moreover, the 3:1 ratio of left to right lung uptake seen immediately after injection was maintained (Figure 4A).

MSC redistribution was predominantly to the liver (48.2 ± 18% at day 2 of initial left lung uptake) in both infarcted and noninfarcted animals (Figure 3D to 3F). ^{111}In oxine alone also demonstrated an increased liver uptake on day 2 (Figure 4B). Kidney uptake remained constant (16.2 ± 21% immediately after injection versus 16.9 ± 8% at day 2), whereas splenic uptake

increased (2.3 ± 2.7% versus 5.6 ± 1.9%). Thus, at 24 hours after MSC injection, loss of MSCs from the lungs and redistribution to organs of the reticuloendothelial system as well as the kidney and bone marrow occurred (Figure 4B). Volume-rendered SPECT/CT movies showing the redistribution of the MSCs at 24 hours after injection to the liver in representative infarcted and noninfarcted animals can be viewed in the online-only Data Supplement (Movies III and IV, respectively).

Image pixel values beyond day 2 in the lungs, liver, kidneys, spleen, and heart were found to decline over time at a rate faster than predicted by radioactive decay (Figure 4B and 4c). Because no increase in uptake was observed in these organs after day 3, declines larger than attributable to radioactive decay are likely due to stem cell loss[6] or loss of the radiotracer from the cell.[35,36]

Evidence of Trafficking of MSCs to the Heart

At 24 hours after injection, cardiac uptake in the anterior apex without decay correction was not significantly different than immediately after injection (4.1 ± 3.5% of day 1 left lung uptake on day 1 versus 4.6 ± 2.4% on day 2), indicating redistribution of MSCs to the heart well beyond that expected by the normal radioactive decay (Figure 4C). In contrast, the cardiac uptake in the noninfarcted animal demonstrated the expected exponential decay from day 1 to day 2 on the basis of the ^{111}In oxine half-life (data not shown).

Curiously, an intense focal uptake in a more anterior midventricular location in the infarcted myocardium was clearly visualized in half of the infarcted dogs receiving MSCs. This cardiac "hot spot" was best visualized at day 2 because of substantial clearance of lung uptake (181 ± 240% of day 1 left lung uptake; Figure 5B). However, with the use of our specialized quantitative SPECT image reconstruction method,[26–30] spillover from the lung, which could be misinterpreted as cardiac uptake, was avoided such that the cardiac hot spot could also be observed at initial injection in these same animals (189 ± 160% of day 1 left lung uptake; Figure 5A). This focal cardiac uptake was also apparent in half of the infarcted animals (Movie III) but not in the noninfarcted animal (Movie IV). Activity time curves indicated that the hot spot decreased more rapidly than could be attributed strictly to radioactive decay (Figure 4D).

However, in all of the infarcted animals receiving MSCs, image pixel values in the anterior apex, excluding the cardiac hot spot if present at day 1, were increased after day 1 in infarcted tissue relative to noninfarcted tissue (3.03 ± 2.9% infarcted versus 1.38 ± 2.2% noninfarcted of day 1 left lung; $P < 0.02$). In the noninfarcted animal receiving ^{111}In oxine–labeled MSCs, no differential cardiac uptake was observed between the anterior and inferior myocardium (2.56 ± 1.9% versus 1.95 ± 1.4%; $P = 0.19$).

At later time points of 4 to 7 days after MSC injection, a diffuse myocardial uptake, not related to the original focal cardiac hot spot if present, could be observed in all infarcted animals corresponding to the anterior apical distribution of the MI (Figure 5D to 5F). Volume-rendered SPECT/CT movies demonstrating the apical cardiac uptake in an infarcted animal and the lack of MSCs in the heart in a noninfarcted animal at 5 to 7 days after injection may be viewed in the online-only Data Supplement (Movies V and VI, respectively).

Infarct Size by MRI

Infarct size at approximately 1 week after infarction was 18.8 ± 6.8% of left ventricular mass. The site of MI overlapped areas of focal uptake in the heart on SPECT images (Figure 6). No MRI evidence of Feridex-PLL–labeled MSCs, which would appear as a hypointense lesions,[23] could be detected in the heart by either in vivo or postmortem MRI (data not shown).

Accuracy of Emission Data

Tissue counts correlated well with quantitative SPECT data (R^2 = 0.66; Figure 7A). This high agreement is due in part to the quantitative SPECT image reconstruction methods that compensate for image degradation effects and also diminish internal effects from organs with high activity, such as the liver, that might contaminate adjacent organs, such as the heart (Figure I in the online-only Data Supplement).

The accuracy of our quantitative SPECT image reconstruction methods[26–30] was further confirmed by a high agreement between the calculated and actual injected dose (R^2 = 0.96; y = 0.99x + 11.9; Figure 7B). On successive days after injection, decreasing amounts of the original dose could be accounted for at successive imaging sessions (91 ± 16% on day 1; 83 ± 21% on day 2; 71 ± 7% on days 4 to 8; Figure 7C).

On the basis of well counter tissue data, the estimated number of MSCs retained in the infarcted myocardium at ≈1 week after injection was 3180.8 ± 1271 per gram of nonviable myocardium. If it is assumed that the MSCs were distributed equally throughout the infarcted tissue, then, on average, 81 500 MSCs were localized in each infarcted heart at animal sacrifice ≈1 week after MSC injection.

Histological Analysis

Prussian blue–positive staining representing iron, presumably from Feridex labeling of the MSCs, was detected in the infarcted heart, liver, spleen, and lung (Figure 8A to 8D). In particular, MSCs were localized in the peri-infarction zone and MI (Figure 8E and 8F). No Prussian blue–positive cells were detected in the remote noninfarcted heart or the kidney (Figure 8G to 8I). Fluorescent imaging demonstrated a similar pattern with cell tracker orange (Figure II in the online-only Data Supplement). Because the Prussian blue–positive cells could potentially represent phagocytic macrophages that either contain native iron or have ingested Feridex from lysed MSCs, enzymatic histochemistry was performed to detect macrophages. Although macrophages were present in infarcted myocardium, the majority of Prussian blue–positive cells were intact Feridex-labeled MSCs (Figure 8J and 8K) that did not colabel with the acid phosphatase enzyme (ie, red). Moreover, the immunofluorescent staining of the dextran coating in Feridex also demonstrated that the cells contained the original magnetic label on an adjacent section (Figure 8L). No multinucleated Prussian blue–positive cells were noted, indicating little to no cell fusion with native cells. At 1 week after injection, little to no differentiation of MSCs would be expected,[18] and thus no immunohistochemical studies were performed to determine whether the MSCs had undergone differentiation.

Discussion

In the present study we have demonstrated that ^{111}In oxine, a Food and Drug Administration–approved clinical radiotracer for autologous leukocyte labeling, can also be used to efficiently label MSCs to study their dynamic biodistribution and trafficking after an intravenous injection. One advantage of ^{111}In oxine is the relatively long half-life, which allows for serial imaging. In the present study we were able to use a specialized SPECT reconstruction technique[29,30] to quantitatively track cell distribution with <12 μCi error in the whole-body dose and >70% of the dose still accounted for at ≈1 week, which is in agreement with previous reports on elution of the radiotracer.[35,36]

Systemic administration of stem cells offers a minimally invasive route for delivery that is especially attractive for multiple dosing regimens. However, because of the relatively large size (≈25 μm in suspension) of MSCs, radiolabeled studies of ^{111}In oxine–labeled MSCs have shown high initial uptake in the lung after intravenous injection,[19,20] which may lead to

undesirable side effects. On the other hand, ^{111}In oxine–labeled human endothelial progenitor cells (EPCs), which are substantially smaller than MSCs, demonstrated little lung uptake after systemic injection.[37] However, when ^{111}In oxine–labeled human hematopoietic progenitor cells (HPCs) were injected intraventricularly in the same rat infarction model,[35] a transient high uptake in the lungs, which resolved by 24 hours after injection, was observed.

In addition, prior studies with ^{111}In oxine–labeled MSCs have shown a species-dependent redistribution after intravenous injection.[19–21] In the noninfarcted rat, planar gamma camera imaging showed redistribution to the liver at 48 hours after injection with relatively high uptake persisting in the lung.[19] In a closed-chest swine reperfused MI model, ^{111}In oxine–labeled MSCs administered intravenously resulted in persistent localization of the MSCs in the lungs with minimal redistribution to other organs such as the liver and spleen at follow-up intervals of up to 2 weeks.[20] Moreover, no localized uptake of the radiolabeled MSCs in the infarcted heart was demonstrated.[20] On the other hand, in an open-chest rat MI model, a systemic injection containing ≈50% purified MSCs labeled with technetium 99m showed uptake not only in the lung but also in the liver, spleen, and heart.[21] Because of the nontomographic nature of the imaging, localization of the MSCs in the infarcted heart in this rat model could only be demonstrated by histology. Similarly, localization of EPCs to the heart in the rat was modest and was best demonstrated histologically.[37] HPCs showed no cardiac localization in this same rat model.[35]

Although ^{111}In oxine labeling of EPCs did not appear to affect viability, functionality, or migratory capacity, HPC labeling reportedly severely impaired migratory and proliferative capacity as well as overall viability and functionality. However, it is impossible to determine whether an increased radiosensitivity of HPCs to ^{111}In oxine is the sole result of a less differentiated cell type or reflects the effects of a different radiation dose and long-term freezing of HPCs relative to, for example, EPCs. In the present study allogeneic canine MSCs were all frozen before ^{111}In oxine labeling, yet in vitro assays demonstrated high viability with only slight declines, if any, in proliferative or metabolic activity in MSCs labeled up to labeling doses of 30 μCi per million MSCs. In vitro differentiation capacity of the MSCs was not impaired at any dose up to 30 μCi per million MSCs. Moreover, high viability with rapid redistribution after intravenous administration, including evidence of MSC trafficking to MI, was present in vitro. Thus, the present study suggests that MSCs, despite either mechanical trapping and/or adhesion initially in the lungs, receive the appropriate cues to migrate to injured tissue even after freezing and thawing.

Furthermore, the use of radiotracer labeling has given direct insight into the dynamic redistribution of MSCs in a relevant cardiac injury model. In general, rat infarction models require open-chest surgery and thereby create a large skin wound that may potentiate the ischemic cardiac injury. The closed-chest canine reperfused infarction model, as used in the present study, does not have the confounding variable of potentially creating a large release of cytokines in the surgically injured area, which may enhance stem cell mobilization and homing. Moreover, because of the tomographic nature of SPECT/CT, MSC detection and information about the degree and spatial extent of cardiac localization in vivo could be obtained. When combined with high-resolution MRI, the localization of the MSCs in the infarcted and peri-infarction tissue could be demonstrated, which has not been shown in previous planar imaging studies. Because the present study was performed on standard clinical scanners with Food and Drug Administration-approved agents, these techniques could be readily applied to future human clinical trials.

Interestingly, the present study showed redistribution of the allogeneic canine MSCs from an initial high lung uptake to the infarcted heart, liver, spleen, and spine, whereas our previous study using ^{111}In oxine–labeled allogeneic swine MSCs in a reperfused MI showed persistent

lung uptake and no evidence of myocardial homing.[20] Thus, one might conclude that the chemotactic cues may not only be cell line specific, eg, EPCs versus HPCs, but also species specific, eg, swine versus canine. However, a critical factor is to determine whether the ^{111}In oxine labeling adversely affects viability, functionality, migration, and proliferative capacity differently in distinct cell populations as well as species. Further studies are needed to resolve these questions.

Early studies demonstrated that 5 to 20 μCi ^{111}In oxine per 100 million lymphocytes did not cause radiotoxicity in this extremely radiosensitive cell line.[38] Using rat MSCs, Gao and colleagues[19] demonstrated that cell viability and proliferative capacity were not adversely affected at levels up to 40 μCi ^{111}In oxine per million cells, which is in agreement with the in vitro assays used in the present study, indicating that MSCs are less radiosensitive than lymphocytes. The activity used in the present in vivo study was well below this dose at <10 μCi per million MSCs. However, in the peripheral delivery of swine MSCs[20] and rat EPCs[35] in animal MI models, labeling was performed at a much higher level of radioactivity (100 to 810 μCi per million cells). Although viability of the swine MSCs remained >95% for 48 hours after labeling, viability was reduced after 48 hours in the human EPCs. Thus, it is possible that the lack of homing and redistribution seen in the previous studies could be largely due to the effect of the label, ie, radioactivity or perhaps the oxine portion of the label, rather than any specific mechanism related to cell type or species. Therefore, in considering ^{111}In oxine labeling of human stem cells, the effect of radiation dose on human cell lines will need to be carefully assessed before clinical trials are initiated. Accordingly, the homing and redistribution of the ^{111}In oxine–labeled MSCs used in the present study indicate that migratory capacity in vivo is not affected at the 5 μCi per million MSCs dosage.

The large redistribution of the ^{111}In oxine–labeled MSCs to the liver at 24 hours after injection was consistent with previous histological studies of intravenous delivery of MSCs in a lethal total-body irradiation nonhuman primate model.[39] ^{111}In oxine–labeled HSCs delivered systemically also demonstrated trafficking to the liver in both irradiated and nonirradiated mice.[40] Similarly, both hematopoietic and nonhematopoietic cells delivered systemically have shown trafficking to the spleen.[38,40,41] However, in one of these studies using bone marrow–derived mononuclear cells and a rat cryoinjury model, localization to the liver based on fluorescent microscopy at 7 days after injection was not observed. Similarly, at 12 to 86 days after whole-body irradiation, Chapel et al[42] were unable to demonstrate enhanced green fluorescent protein–transfected MSCs administered systemically in non-human primates in the liver or spleen by PCR. However, these results may not be inconsistent but rather suggest that PCR and microscopic analyses require a higher threshold of detection than radiolabeling (eg, 10-fold larger number of cells needed by PCR in the heart).[43]

Although intraventricular injections of stem cells have been shown to yield higher stem cell engraftment in the MI, the primary mode of heart localization may be due to leakage or trapping of the stem cells on the first pass through the coronary vasculature rather than redistribution and direct homing of the stem cells to the heart. Similarly, in 50% of the animals in the present study, SPECT/CT revealed a high uptake of MSCs after intravenous injection in the mid-to-basal infarcted region that did not increase over time, which may represent some nonspecific uptake mechanism. However, at 24 hours after injection, a maximal uptake in the infarcted myocardium, in a site distinct from any focal midbasilar uptake noted in half of the animals, was present in all animals on imaging. These results are consistent with the original studies of leukocyte trafficking with the use of ^{111}In oxine labeling in infarcted animals after an intravenous injection. In these leukocyte trafficking studies, there was a window of 24 to 96 hours after MI when leukocyte accumulation occurred, suggesting a specific uptake mechanism.[44] Thus, the increased uptake at day 1 (or 96 hours after MI) of ^{111}In oxine–labeled canine MSCs in the present study indicates that shared migratory cues for leukocytes and MSCs

are present in the first days after MI. Moreover, the lack of cardiac uptake in the infarcted animal that received free ^{111}In oxine indicates that the increased cardiac signal observed with SPECT in the dogs receiving exogenous MSCs reflects cellular distribution rather than just tracer uptake.

The inability to detect MSC engraftment by MRI was consistent with previous studies that have shown an MRI detection limit at clinical field strengths of cell numbers >10^5 for Feridex-PLL–labeled cells in the heart.[45,46] Although the number of cells that were found to engraft in the heart at 1 week after injection was low, our results are consistent with previous studies indicating that a low number of cells survive beyond 24 hours after administration.[6,18,35] However, the noninvasive nature of intravenous delivery offers promise as a method for serial administration of MSCs to increase engraftment.

Thus, in the present study we have presented a method to dynamically track the whole-body redistribution of MSCs after systemic injection. In addition, radiolabeling methods to monitor stem cell trafficking may be more sensitive than immunofluorescent or quantitative techniques such as PCR, which can only be performed as a single “snapshot” either postmortem or in limited tissue obtained after biopsy. In particular, we have demonstrated a method to monitor the in vivo engraftment of <100 000 MSCs in the infarcted heart using imaging scanners and 2 FDA-approved agents that are currently available in most major clinical centers. Thus, important questions such as identifying the factors involved in stem cell homing as well as the time course of the expression of these factors could be monitored in vivo to develop methods to optimize therapeutic protocols for enhanced stem cell engraftment.

Supplementary Material

Refer to Web version on PubMed Central for supplementary material.

Acknowledgements

This work was funded in part by NIH grants R01-HL6563439, R01-HL73223 (Drs Kraitchman, Gilson, and Bulte), K02-HL05193 (Dr Kraitchman), RO1-NS045062 (Dr Bulte), and R01-EB 000168 (Dr Tsui), DOD research grant DAMD17-02-1-0112 (Dr Tsui), and Defense Advanced Research Projects Agency grant N66001-02-C-8086 (Dr Pittenger). The authors thank James Engles, BS, for assistance in radioactive cell labeling, Xide Zhao for assistance in SPECT image reconstruction, and O’Bod Nicely, CNMT, and David Clough, CNMT, for assistance with SPECT/CT image acquisition.

References

1. Kocher AA, Schuster MD, Szabolcs MJ, Takuma S, Burkhoff D, Wang J, Homma S, Edwards NM, Itescu S. Neovascularization of ischemic myocardium by human bone-marrow-derived angioblasts prevents cardiomyocyte apoptosis, reduces remodeling and improves cardiac function. Nat Med 2001;7:430–436. [PubMed: 11283669]
2. Bittner RE, Schofer C, Weipoltshammer K, Ivanova S, Streubel B, Hauser E, Freilinger M, Hoger H, Elbe-Burger A, Wachtler F. Recruitment of bone-marrow-derived cells by skeletal and cardiac muscle in adult dystrophic mdx mice. Anat Embryol (Berl) 1999;199:391–396. [PubMed: 10221450]
3. Britten MB, Abolmaali ND, Assmus B, Lehmann R, Honold J, Schmitt J, Vogl TJ, Martin H, Schachinger V, Dimmeler S, Zeiher AM, Teupe C, Britten M, Dobert N, Grunwald F, Aicher A, Urbich C, Hoelzer D. Infarct remodeling after intracoronary progenitor cell treatment in patients with acute myocardial infarction (TOPCARE-AMI): mechanistic insights from serial contrast-enhanced magnetic resonance imaging. Circulation 2003;108:2212–2218. [PubMed: 14557356]
4. Bittira B, Shum-Tim D, Al-Khaldi A, Chiu RC. Mobilization and homing of bone marrow stromal cells in myocardial infarction. Eur J Cardiothorac Surg 2003;24:393–398. [PubMed: 12965310]
5. Orlic D, Kajstura J, Chimenti S, Limana F, Jakoniuk I, Quaini F, Nadal-Ginard B, Bodine DM, Leri A, Anversa P. Mobilized bone marrow cells repair the infarcted heart, improving function and survival. Proc Natl Acad Sci U S A 2001;98:10344–10349. [PubMed: 11504914]

6. Shake JG, Gruber PJ, Baumgartner WA, Senechal G, Meyers J, Redmond JM, Pittenger MF, Martin BJ. Mesenchymal stem cell implantation in a swine myocardial infarct model: engraftment and functional effects. Ann Thorac Surg 2002;73:1919–1925. [PubMed: 12078791]discussion 1926.
7. Tomita S, Li RK, Weisel RD, Mickle DA, Kim EJ, Sakai T, Jia ZQ. Autologous transplantation of bone marrow cells improves damaged heart function. Circulation 1999;100(suppl):II247–II256. [PubMed: 10567312]
8. Oh H, Bradfute SB, Gallardo TD, Nakamura T, Gaussin V, Mishina Y, Pocius J, Michael LH, Behringer RR, Garry DJ, Entman ML, Schneider MD. Cardiac progenitor cells from adult myocardium: homing, differentiation, and fusion after infarction. Proc Natl Acad Sci U S A 2003;100:12313–12318. [PubMed: 14530411]
9. Assmus B, Schachinger V, Teupe C, Britten M, Lehmann R, Dobert N, Grunwald F, Aicher A, Urbich C, Martin H, Hoelzer D, Dimmeler S, Zeiher AM. Transplantation of Progenitor Cells and Regeneration Enhancement in Acute Myocardial Infarction (TOPCARE-AMI). Circulation 2002;106:3009–3017. [PubMed: 12473544]
10. Wollert KC, Meyer GP, Lotz J, Ringes-Lichtenberg S, Lippolt P, Breidenbach C, Fichtner S, Korte T, Hornig B, Messinger D, Arseniev L, Hertenstein B, Ganser A, Drexler H. Intracoronary autologous bone-marrow cell transfer after myocardial infarction: the BOOST randomised controlled clinical trial. Lancet 2004;364:141–148. [PubMed: 15246726]
11. Deb A, Wang S, Skelding KA, Miller D, Simper D, Caplice NM. Bone marrow–derived cardiomyocytes are present in adult human heart: a study of gender-mismatched bone marrow transplantation patients. Circulation 2003;107:1247–1249. [PubMed: 12628942]
12. Bayes-Genis A, Salido M, Sole Ristol F, Puig M, Brossa V, Camprecios M, Corominas JM, Marinoso ML, Baro T, Vela MC, Serrano S, Padro JM, Bayes de Luna A, Cinca J. Host cell-derived cardiomyocytes in sex-mismatch cardiac allografts. Cardiovasc Res 2002;56:404–410. [PubMed: 12445881]
13. Muller P, Pfeiffer P, Koglin J, Schafers HJ, Seeland U, Janzen I, Urbschat S, Bohm M. Cardiomyocytes of noncardiac origin in myocardial biopsies of human transplanted hearts. Circulation 2002;106:31–35. [PubMed: 12093766]
14. Hruban RH, Long PP, Perlman EJ, Hutchins GM, Baumgartner WA, Baughman KL, Griffin CA. Fluorescence in situ hybridization for the Y-chromosome can be used to detect cells of recipient origin in allografted hearts following cardiac transplantation. Am J Pathol 1993;142:975–980. [PubMed: 7682765]
15. Laflamme MA, Myerson D, Saffitz JE, Murry CE. Evidence for cardiomyocyte repopulation by extracardiac progenitors in transplanted human hearts. Circ Res 2002;90:634–640. [PubMed: 11934829]
16. Sauer H, Hescheler J, Wartenberg M. Cardiac differentiation of mesenchymal stem cells in sex mismatched transplanted hearts: self-repair or just a visit? Cardiovasc Res 2002;56:357–358. [PubMed: 12445876]
17. Pittenger MF, Mackay AM, Beck SC, Jaiswal RK, Douglas R, Mosca JD, Moorman MA, Simonetti DW, Craig S, Marshak DR. Multilineage potential of adult human mesenchymal stem cells. Science 1999;284:143–147. [PubMed: 10102814]
18. Toma C, Pittenger MF, Cahill KS, Byrne BJ, Kessler PD. Human mesenchymal stem cells differentiate to a cardiomyocyte phenotype in the adult murine heart. Circulation 2002;105:93–98. [PubMed: 11772882]
19. Gao J, Dennis JE, Muzic RF, Lundberg M, Caplan AI. The dynamic in vivo distribution of bone marrow-derived mesenchymal stem cells after infusion. Cell Tissues Organs 2001;169:12–20.
20. Chin BB, Nakamoto Y, Bulte JW, Pittenger MF, Wahl R, Kraitchman DL. ^{111}In oxine labelled mesenchymal stem cell SPECT after intravenous administration in myocardial infarction. Nucl Med Commun 2003;24:1149–1154. [PubMed: 14569169]
21. Barbash IM, Chouraqui P, Baron J, Feinberg MS, Etzion S, Tessone A, Miller L, Guetta E, Zipori D, Kedes LH, Kloner RA, Leor J. Systemic delivery of bone marrow-derived mesenchymal stem cells to the infarcted myocardium: feasibility, cell migration, and body distribution. Circulation 2003;108:863–868. [PubMed: 12900340]

22. Frank JA, Miller BR, Arbab AS, Zywicke HA, Jordan EK, Lewis BK, Bryant LH Jr, Bulte JWM. Clinically applicable labeling of mammalian and stem cells by combining superparamagnetic iron oxides and transfection agents. Radiology 2003;228:480–487. [PubMed: 12819345]
23. Kraitchman DL, Heldman AW, Atalar E, Amado L, Martin BJ, Pittenger MF, Hare JM, Bulte JW. In vivo magnetic resonance imaging of mesenchymal stem cells in myocardial infarction. Circulation 2003;107:2290–2293. [PubMed: 12732608]
24. Malich G, Markovic B, Winder C. The sensitivity and specificity of the MTS tetrazolium assay for detecting the in vitro cytotoxicity of 20 chemicals using human cell lines. Toxicology 1997;124:179–192. [PubMed: 9482120]
25. Kostura L, Kraitchman DL, Mackay AM, Pittenger MF, Bulte JW. Feridex labeling of mesenchymal stem cells inhibits chondrogenesis but not adipogenesis or osteogenesis. NMR Biomed 2004;17:513–517. [PubMed: 15526348]
26. Tsui BM, Gullberg GT, Edgerton ER, Ballard JG, Perry JR, McCartney WH, Berg J. Correction of nonuniform attenuation in cardiac SPECT imaging. J Nucl Med 1989;30:497–507. [PubMed: 2786944]
27. Frey EC, Tsui BMW. T. Modeling the scatter response function in inhomogeneous scattering media for SPECT. IEEE Trans Nucl Sci 1994;41:1585–1593.
28. Tsui BMW, Hu HB, Gilland DR, Gullberg GT. Implementation of simultaneous attenuation and detector response correction in SPECT. IEEE Trans Nucl Sci 1988;NS-35:778–783.
29. Tsui BMW, Zhao XD, Frey EC, McCartney WH. Quantitative single-photon emission computed tomography: basics and clinical considerations. Semin Nucl Med 1994;XXIV:38–65. [PubMed: 8122128]
30. Kadrmas DJ, Frey EC, Karimi SS, Tsui BM. Fast implementations of reconstruction-based scatter compensation in fully 3D SPECT image reconstruction. Phys Med Biol 1998;43:857–873. [PubMed: 9572510]
31. Loening AM, Gambhir SS. AMIDE: a free software tool for multimodality medical image analysis. Mol Imaging 2003;2:131–137. [PubMed: 14649056]
32. Judd RM, Lugo-Olivieri CH, Arai M, Kondo T, Croisille P, Lima JA, Mohan V, Becker LC, Zerhouni EA. Physiological basis of myocardial contrast enhancement in fast magnetic resonance images of 2-day-old reperfused canine infarcts. Circulation 1995;92:1902–1910. [PubMed: 7671375]
33. Amado LC, Kraitchman DL, Gerber BL, Castillo E, Boston RC, Grayzel J, Lima JA. Reduction of “no-reflow” phenomenon by intra-aortic balloon counterpulsation in a randomized magnetic resonance imaging experimental study. J Am Coll Cardiol 2004;43:1291–1298. [PubMed: 15063444]
34. Bulte JW, Arbab AS, Douglas T, Frank JA. Preparation of magnetically labeled cells for tracking by magnetic resonance imaging. Methods Enzymol 2004;386:275–299. [PubMed: 15120257]
35. Brenner W, Aicher A, Eckey T, Massoudi S, Zuhayra M, Koehl U, Heeschen C, Kampen WU, Zeiher AM, Dimmeler S, Henze E. ^{111}In-labeled CD34+ hematopoietic progenitor cells in a rat myocardial infarction model. J Nucl Med 2004;45:512–518. [PubMed: 15001696]
36. Kuyama J, McCormack A, George AJ, Heelan BT, Osman S, Batchelor JR, Peters AM. Indium-111 labelled lymphocytes: isotope distribution and cell division. Eur J Nucl Med 1997;24:488–496. [PubMed: 9142728]
37. Aicher A, Brenner W, Zuhayra M, Badorff C, Massoudi S, Assmus B, Eckey T, Henze E, Zeiher AM, Dimmeler S. Assessment of the tissue distribution of transplanted human endothelial progenitor cells by radioactive labeling. Circulation 2003;107:2134–2139. [PubMed: 12695305]
38. Chisholm PM, Danpure HJ, Healey G, Osman S. Cell damage resulting from the labeling of rat lymphocytes and HeLa S3 cells with In-111 oxine. J Nucl Med 1979;20:1308–1311. [PubMed: 119830]
39. Devine SM, Cobbs C, Jennings M, Bartholomew A, Hoffman R. Mesenchymal stem cells distribute to a wide range of tissues following systemic infusion into nonhuman primates. Blood 2003;101:2999–3001. [PubMed: 12480709]
40. Cui J, Wahl RL, Shen T, Fisher SJ, Recker E, Ginsburg D, Long MW. Bone marrow cell trafficking following intravenous administration. Br J Haematol 1999;107:895–902. [PubMed: 10606901]

41. Ciulla MM, Lazzari L, Pacchiana R, Esposito A, Bosari S, Ferrero S, Gianelli U, Paliotti R, Busca G, Giorgetti A, Magrini F, Rebulla P. Homing of peripherally injected bone marrow cells in rat after experimental myocardial injury. Haematologica 2003;88:614–621. [PubMed: 12801836]

42. Chapel A, Bertho JM, Bensidhoum M, Fouillard L, Young RG, Frick J, Demarquay C, Cuvelier F, Mathieu E, Trompier F, Dudoignon N, Germain C, Mazurier C, Aigueperse J, Borneman J, Gorin NC, Gourmelon P, Thierry D. Mesenchymal stem cells home to injured tissues when co-infused with hematopoietic cells to treat a radiation-induced multi-organ failure syndrome. J Gene Med 2003;5:1028–1038. [PubMed: 14661178]

43. Pittenger MF, Martin BJ. Mesenchymal stem cells and their potential as cardiac therapeutics. Circ Res 2004;95:9–20. [PubMed: 15242981]

44. Thakur ML, Gottschalk A, Zaret BL. Imaging experimental myocardial infarction with indium-111-labeled autologous leukocytes: effects of infarct age and residual regional myocardial blood flow. Circulation 1979;60:297–305. [PubMed: 445748]

45. Bulte JW, Kraitchman DL. Monitoring cell therapy using iron oxide MR contrast agents. Curr Pharm Biotechnol 2004;5:567–584. [PubMed: 15579045]

46. Hill JM, Dick AJ, Raman VK, Thompson RB, Yu ZX, Hinds KA, Pessanha BS, Guttman MA, Varney TR, Martin BJ, Dunbar CE, McVeigh ER, Lederman RJ. Serial cardiac magnetic resonance imaging of injected mesenchymal stem cells. Circulation 2003;11:11.

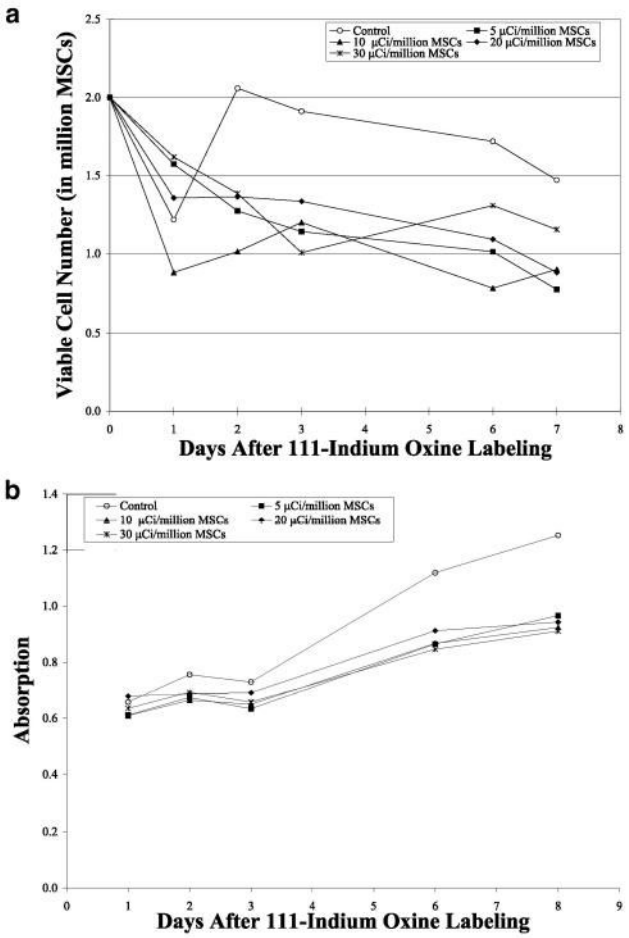

Figure 1.

a, Viable cell counts from in vitro assay of either unlabeled MSCs (control) or MSCs labeled with increasing doses of ^{111}In oxine ranging from 5 to 30 μCi per million MSCs determined 1 to 7 days after labeling. Cells were initially plated in a T-25 flask at a density of 2×10^6 MSCs. Cell counts were determined every other day in alternate flasks. Cell counts remained constant after adhering ≈48 hours after seeding. b, MTS assay measuring absorption of different doses of ^{111}In oxine–labeled MSCs and unlabeled MSCs (control) at 1 to 8 days after labeling. At 6 days after labeling, unlabeled MSCs showed an increased metabolic activity relative to labeled cells (*$P < 0.001$). However, no dose-dependent change in metabolic activity was noted between different amounts of MSC radiolabeling.

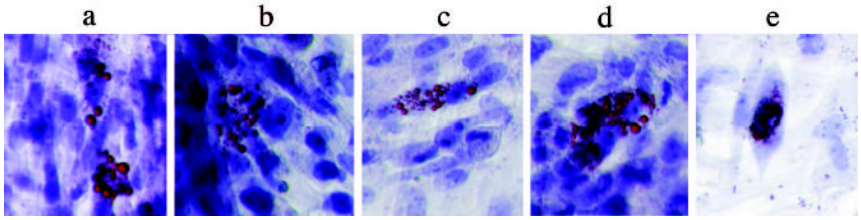

Figure 2.

Adipogenic differentiation of MSCs in vitro was confirmed with Oil Red O staining, in which lipid vacuoles stain red. Both unlabeled (a) and ^{111}In oxine–labeled MSCs (b = 5; c = 10; d = 20; and e = 30 μCi/million MSCs) showed equivalent ability to differentiate.

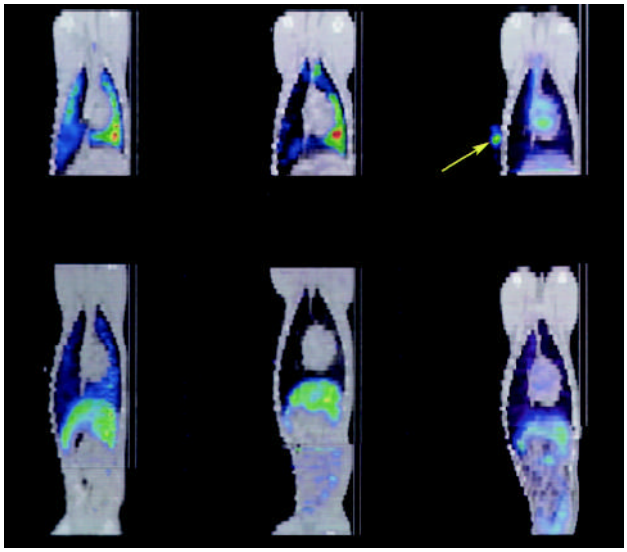

Figure 3.
Coronal fused SPECT (color) and CT (gray-scale) image of a dog with (top left) and without (top middle) MI during the first hours after intravenous injection of ^{111}In oxine–labeled MSCs showing predominant lung uptake with increased uptake to the dependent left lung (green-yellow color toward right). In a dog with MI that received ^{111}In oxine without MSCs (top right), the tracer behaves primarily as a blood pool agent, with uptake visible in left and right ventricles of the heart. A reference marker (arrow) containing ^{111}In oxine was placed on the chest wall on the dog that did not receive MSCs (top right). Redistribution of ^{111}In oxine–labeled MSCs to predominantly the liver occurs at 24 hours after intravenous injection in both a representative infarcted (bottom left) and noninfarcted (bottom middle) dog. In an infarcted dog injected intravenously with ^{111}In oxine only (ie, no MSCs), a similar pattern of redistribution to the liver is observed at 24 hours after injection (bottom right).

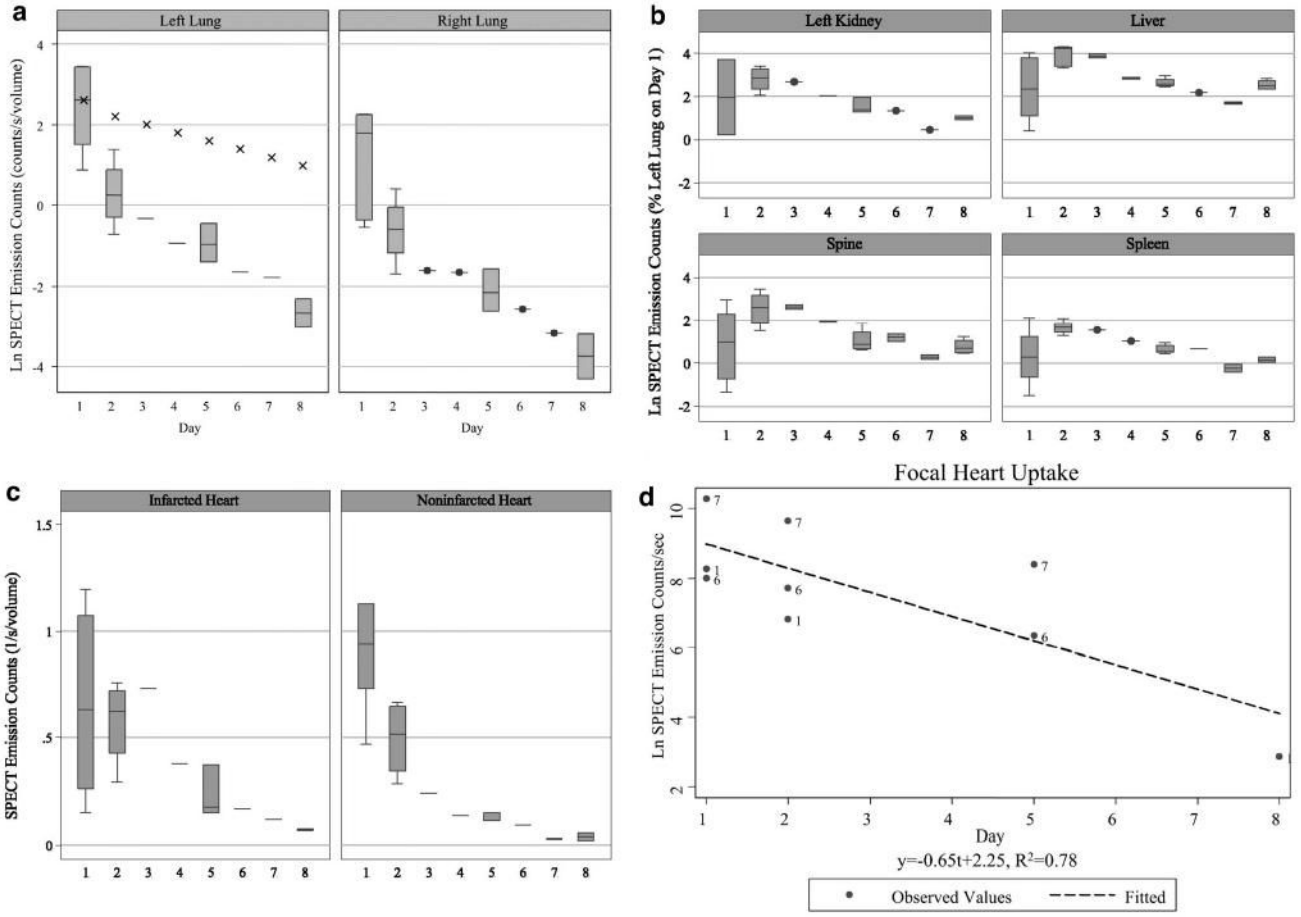

Figure 4.

a, Box-whisker plot of natural log of lung emission counts by imaging day. Initially, more radiolabeled MSCs are present in the left lung (left) than the right lung (right) because of the injection being performed with the animal on the left side (ie, dependent lung uptake). The lung emission counts over time decay faster than predicted by radioactive decay alone (eg, linear decay shown as crosses), indicating either redistribution of MSCs to other organs or cell death and removal. b, Uptake of ^{111}In oxine–labeled MSCs increased in the kidney, liver, spine, and spleen at 24 hours after injection (day 2). After day 3, the uptake decreased at a rate faster than the radioactive decay of ^{111}In oxine, indicating cell loss or loss of tracer. c, Activity in the infarcted anterior apex of the heart (left) was relatively constant for the first 24 hours after injection, indicating redistribution of ^{111}In oxine–labeled MSCs to the infarcted tissue, whereas a rapid decrease in activity in the noninfarcted myocardium (right) was observed in the first 24 hours after injection, indicating a combination of radioactive decay plus loss of MSCs in normal heart tissue. d, In 3 animals demonstrating a focal uptake of activity to the heart, the decay of the activity was ≈3 times faster than predicted for radioactive decay of ^{111}In oxine.

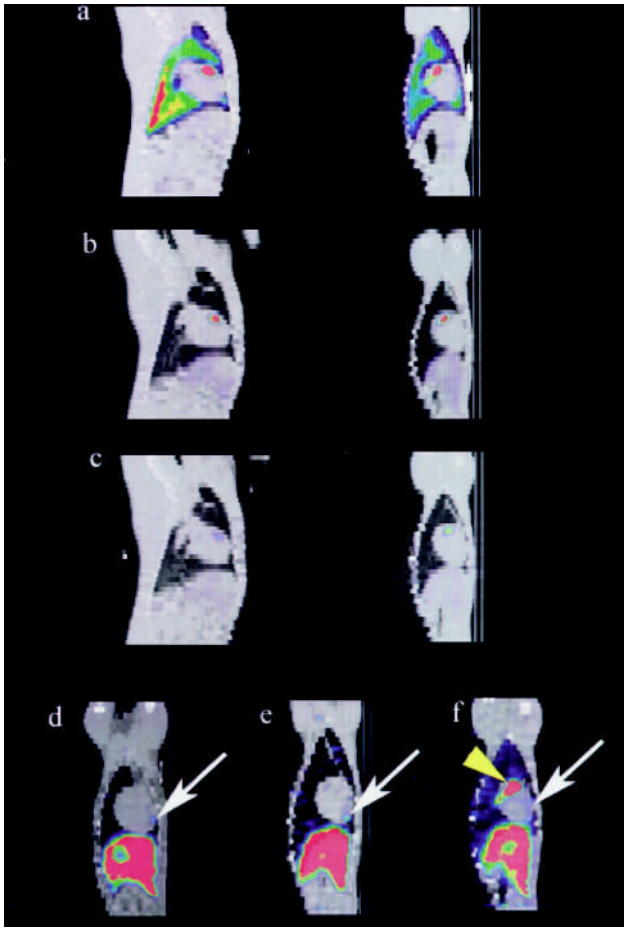

Figure 5.
Sagittal (left) and coronal (right) view of fused SPECT/CT images on days 1 (a), 2 (b), and 7 (c) in an animal that demonstrated focal uptake in the anterior midventricular region of the heart. d to f, At the last imaging time point (days 5 to 8), an anterior apical region of MSC uptake (arrow) is shown in 3 representative animals in the coronal view. This more anterior apical distribution was present independent of whether an early focal hot spot was observed (yellow arrowhead, f only).

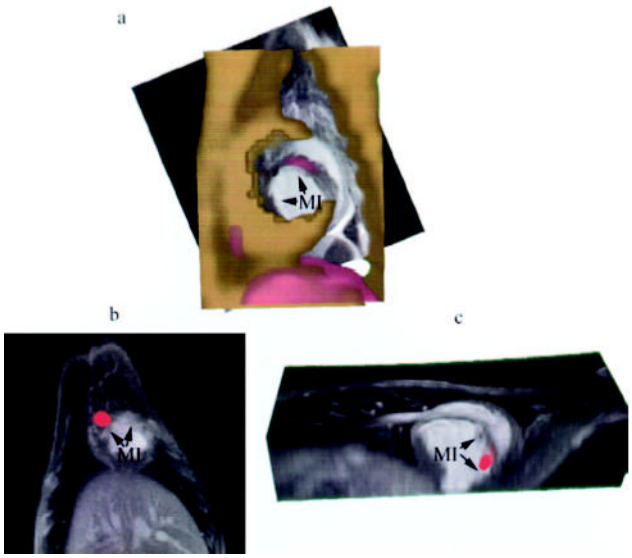

Figure 6.

Registration of SPECT/CT with MR images of the heart demonstrating focal uptake of MSCs in the peri-infarcted region. a, Short-axis view of alignment of CT (gold) with MRI (gray scale) and SPECT (red) showing focal uptake in the septal region of the MI in a representative dog. b, Focal uptake on SPECT (red) in another animal demonstrating localization of the MSCs to the infarcted myocardium (MI) in the short-axis (b) and long-axis (c) views.

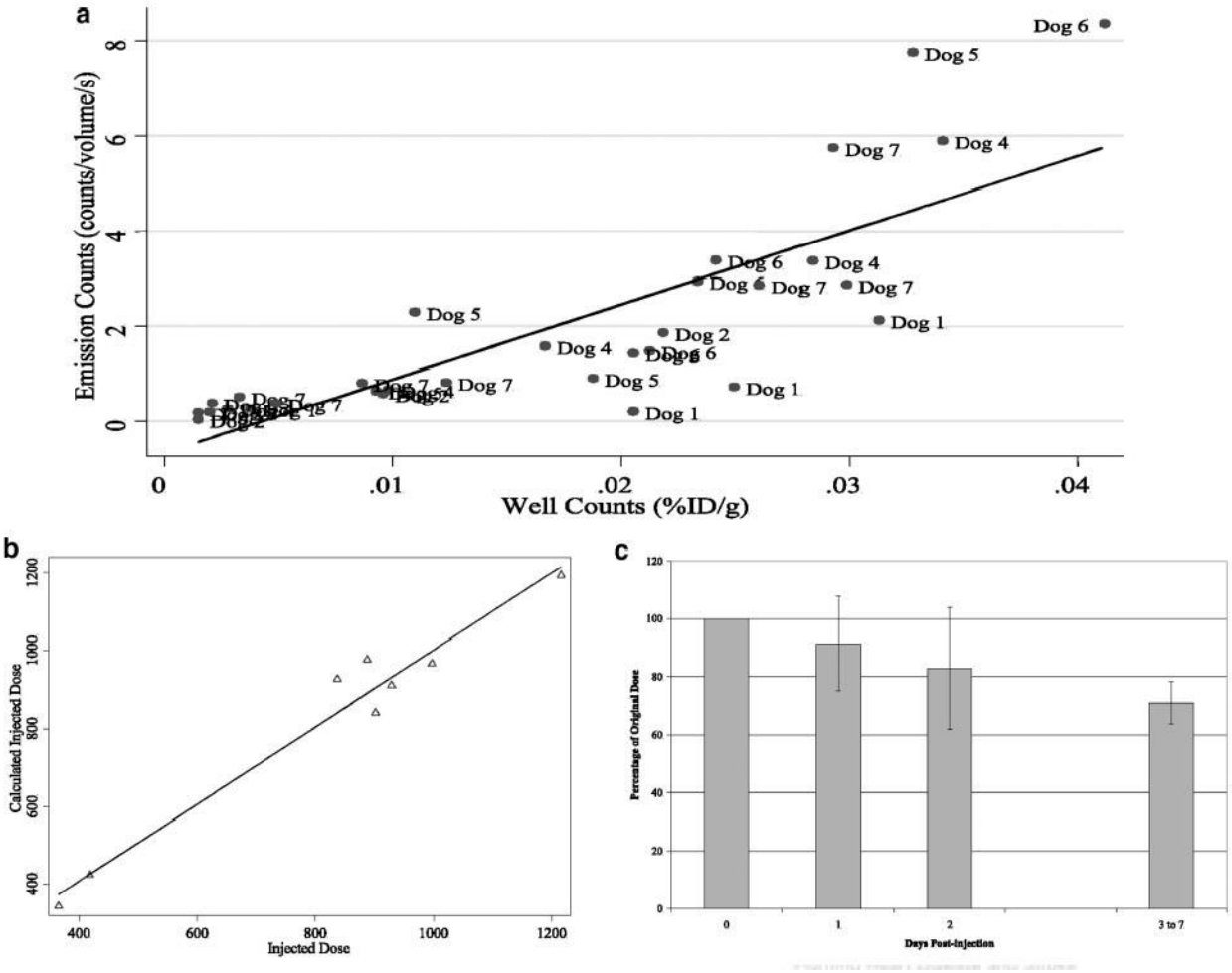

Figure 7.

a, Correlation between SPECT emission counts and gamma well counts from spleen, liver, lung, kidney, and heart. Predicted robust regression (solid line) demonstrates high agreement between quantitative SPECT imaging and tissue gamma well counting ($y = 156.1x - 0.67$; $R^2 = 0.66$). b, Actual injected dose to the calculated injected dose (linear regression: $y = 0.99x + 11.9$; $R^2 = 0.96$) showing ≈12 μCi error in measurement with the use of our specialized reconstruction technique. c, Percentage of the original injected radio-tracer dose that can be accounted for in the whole body after decay correction. After 1 to 2 half-lives, ≈71% of the original dose is retained within the body.

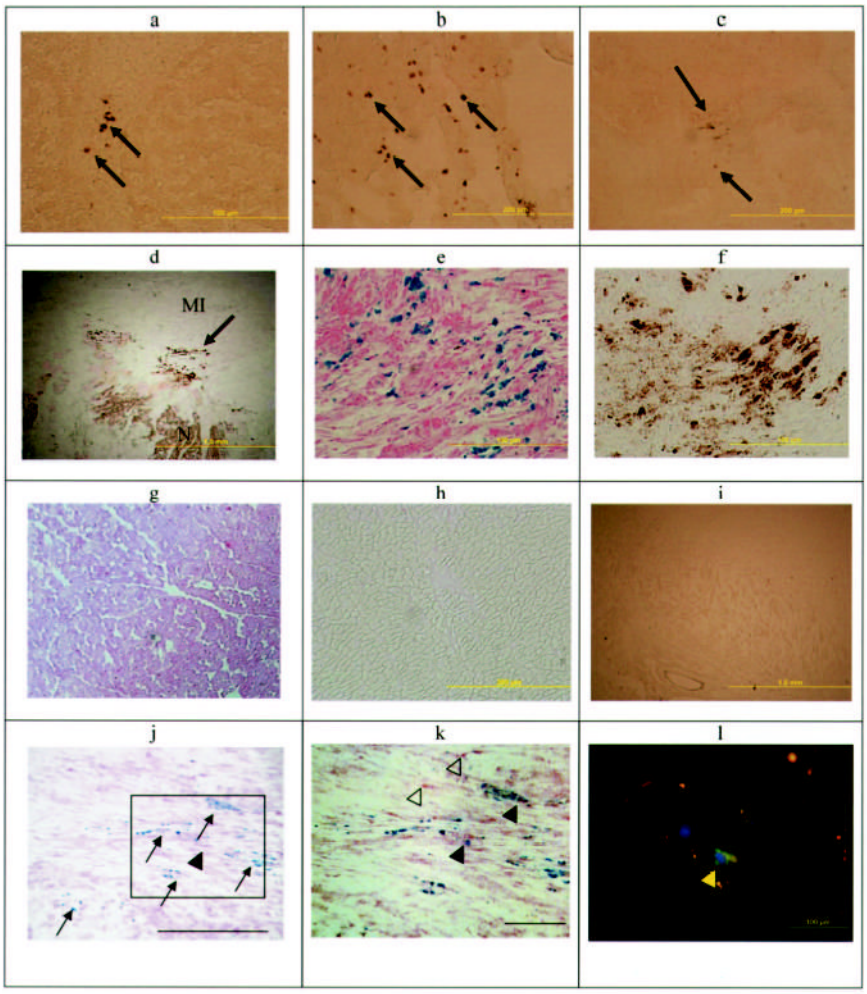

Figure 8.

Photomicrographs of various organs demonstrating the presence or absence of Feridex-labeled MSCs. DAB-enhanced Prussian blue–stained photomicrographs of liver (a), lung (b), spleen (c), and heart (d) demonstrate iron-positive cells in these organs. Higher magnification of d showing Prussian blue staining with (e) and without (f) DAB enhancement demonstrates the intracytoplasmic iron and MSC localization in the MI rim (N indicates normal myocardium). No iron-positive cells were demonstrated with or without DAB-enhanced Prussian blue staining in the noninfarcted myocardium (g, h) or kidney (i). j, Double-staining cells for acid phosphatase (red) and iron (blue) indicate that macrophages (arrowhead) in the heart were rare, whereas the majority of Prussian blue–positive cells were the original Feridex-PLL–labeled MSCs (arrows) (bar = 200 μm). k, Inset of j at a higher magnification demonstrates primarily MSCs (blue stain) with a few macrophages with (filled arrowheads) and without (open arrowheads) iron (bar = 100 μm). l, Dextran staining (green, yellow arrow) indicates Feridex retention in a labeled MSC in the heart. Nuclei are stained with DAPI (blue).